Water-Assisted Highly Efficient Synthesis of Impurity-Free Single-Walled Carbon Nanotubes

Kenji Hata,*† Don N. Futaba,* Kohei Mizuno, Tatsunori Namai, Motoo Yumura, Sumio Iijima

We demonstrate the efficient chemical vapor deposition synthesis of single-walled carbon nanotubes where the activity and lifetime of the catalysts are enhanced by water. Water-stimulated enhanced catalytic activity results in massive growth of superdense and vertically aligned nanotube forests with heights up to 2.5 millimeters that can be easily separated from the catalysts, providing nanotube material with carbon purity above 99.98%. Moreover, patterned, highly organized intrinsic nanotube structures were successfully fabricated. The water-assisted synthesis method addresses many critical problems that currently plague carbon nanotube synthesis.

Single-walled carbon nanotubes (SWNTs) are a key aspect in the emerging field of nanotechnology; however, large-scale synthesis is still limited because of the difficulties in synthesizing SWNTs. Current synthesis methods suffer from the production of impurities that must be removed through purifications steps, which can damage the nanotubes. Dispersion of SWNTs in solutions for further processing also presents challenges because the smooth-sided tubes readily aggregate and form parallel bundles or ropes as a result of van der Waals interactions. We report a rational yet simple and general synthetic approach that concurrently addresses these problems, in which the activity and lifetime of the catalysts are dramatically enhanced by the addition of a controlled amount of water vapor in the growth atmosphere.

We wanted to find a weak oxidizer that would selectively remove amorphous carbon but would not damage the nanotubes at the growth temperature, because coating of the catalyst particles by amorphous carbon during chemical vapor deposition (CVD) reduces their activity and lifetime (*1*). We found that water acts in promoting and preserving catalytic activity. SWNTs were grown by ethylene CVD by using Ar or He with H_2 that contained a small and controlled amount of water vapor (*2*). Balancing the relative levels of ethylene and water was crucial to maximize catalytic lifetime. Water-assisted growth was successfully carried out on various catalysts that generate SWNTs, including Fe nanoparticles (*3*) from $FeCl_3$ and sputtered metal thin films (Fe, Al/Fe, Al_2O_3/Fe, Al_2O_3/Co) on Si wafers, quartz, and metal foils, which demonstrates the generality of our approach.

Water-stimulated catalytic activity results in the growth of dense and vertically aligned SWNT forests with millimeter-scale height in a 10-min growth time. Our best result to date is 2.5 mm in 10 min (Fig. 1, A and B). In contrast with standard ethylene CVD growth, where the catalysts are only active for about 1 min, a height increase of the forests has been observed after 30 min for water-assisted growth. The SWNT/catalyst weight ratio exceeds 50,000%, more than 100 times as high as that of the high-pressure carbon monoxide (HiPco) process (*4*). Provided that the amount of water is well controlled, growths are highly reproducible.

A close examination (Fig. 1C) at the ledge of the SWNT forest illustrates that the nanotubes are densely packed and vertically aligned from the substrate. Low-resolution transmission electron microscopy (TEM) studies (Fig. 1D) of the as-grown forest reveal the presence of only thin nanotubes and the absence of metallic particles and supporting materials that usually comprise a major constituent of as-grown material. High-resolution TEM studies (Fig. 1E and fig. S1) show that the nanotubes are clean SWNTs free from amorphous carbon and metal particles. We have taken hundreds of high-resolution TEM images, and double- or multi-walled carbon nanotubes (MWNTs) were rarely found. Raman spectra (fig. S2) at 514 nm excitation showed clear radial breathing mode peaks (RBM), which confirmed the existence of SWNTs. The sizes of the SWNTs were estimated from the peaks to be in the range of 1 to 3 nm, in agreement with those measured by TEM.

The SWNT forest structure can be easily removed from the substrate with, for example, a razor blade (movie S1). After removal, the substrate is still catalytically active and can grow SWNT forests again, indicating a root-growth mode and the presence of the catalysts on the substrate. Thermo-gravimetric analysis (TGA) was implemented on 10 mg of the as-grown material (Fig. 2A). No measurable residue remained after heating above 750°C, indicating very high purity. The combustion range of the SWNTs was 550°C to 750°C, with the peak weight reduction occurring at 700°C, a result very similar to that of purified, high-quality SWNTs synthesized by a laser-oven method (*5*). Quantitative elemental analysis with x-ray fluorescence spec-

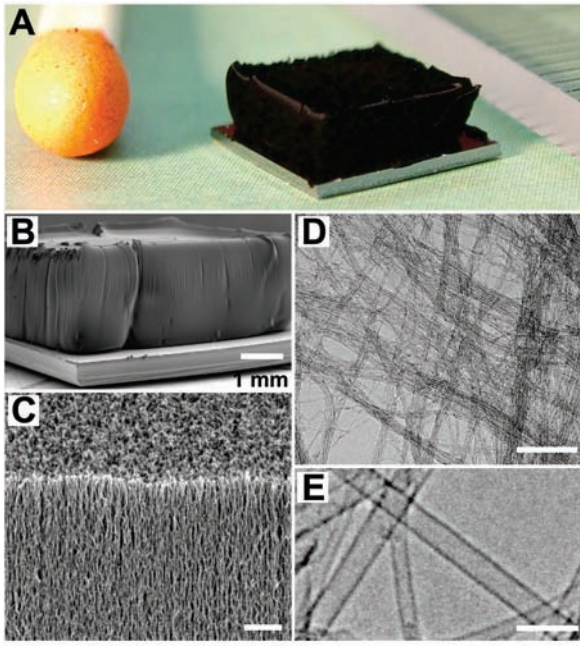

Fig. 1. SWNT forest grown with water-assisted CVD. (**A**) Picture of a 2.5-mm-tall SWNT forest on a 7-mm by 7-mm silicon wafer. A matchstick on the left and ruler with millimeter markings on the right is for size reference. (**B**) Scanning electron microscopy (SEM) image of the same SWNT forest. Scale bar, 1 mm. (**C**) SEM image of the SWNT forest ledge. Scale bar, 1 μm. (**D**) Low-resolution TEM image of the nanotubes. Scale bar, 100 nm. (**E**) High-resolution TEM image of the SWNTs. Scale bar, 5 nm.

Research Center for Advanced Carbon Materials, National Institute of Advanced Industrial Science and Technology (AIST), Tsukuba, 305-8565, Japan.

*These authors contributed equally to this work
†To whom correspondence should be addressed. E-mail: kenji-hata@aist.go.jp

trometry detected 0.013% Fe as the only impurity, meaning carbon purity was more than 99.98%.

Pure SWNTs should allow for the investigation of the intrinsic magnetic properties of SWNTs and for the study of the photoluminescent properties that usually requires dissolution of the SWNTs. For example, a two-dimensional excitation-emission contour plot spectrum (Fig. 3) from preliminary spectrofluorimetric measurements on the as-grown SWNT forest clearly shows discrete spectral peaks. Each peak corresponds to characteristic absorption-emission wavelengths from van Hove optical transitions of SWNTs and can be assigned to specific SWNT structures (*6*). These characteristic peaks have been observed only in individual SWNTs in aqueous micellar suspensions in the past (*6*), and thus the observation of the fluorimetric peaks in the as-grown SWNT forest strongly indicates that the SWNTs are not heavily bundled but that many individual SWNTs exist. Peak locations in the spectrofluorimetric contour plot were mapped out and compared with that of the HiPco tubes (*6*), where a coincidence in peak location was found, which provides additional evidence that the tubes are SWNTs. However, the individual peak intensities differ noticeably from those of the HiPco tubes [e.g., the absence of the peak at 1105-nm emission and 647-nm adsorption wavelengths with assigned tube index (7.6)], which indicates a different abundance distribution of nanotube radii and chiralities. Moreover, a detailed investigation reveals that the spectrofluorimetric contour plot of the SWNT forest is richer in structure than that of the HiPco tubes; we tentatively attribute this result to a wider distribution of nanotubes in our samples. Our results provide a direct route to map the detailed composition of the as-grown SWNT materials and can be adapted to directly study the dependence of the nanotube distribution on the synthesis conditions and catalysts without any ambiguity.

Several additional points and experiments regarding the effect of water deserve comment. First, TGA (Fig. 2B) on pure SWNT material using N_2 gas with water shows that SWNT oxidization starts at about 950°C, which indicates that water does not oxidize and damage SWNTs at the growth temperature. We believe that the small initial weight increase is due to physisorption, supported by the fact that the weight returns to its initial value by subsequent annealing in dry N_2 gas. Second, a black amorphous carbon-coated quartz tube was cleaned transparent by flowing water vapor at 750°C, which provides direct evidence of water-induced oxidation of amorphous carbon. In the literature, hot water on carbon nanotubes has been used to purify amorphous carbon (*7*, *8*). Also, it has been reported that amorphous carbon is effectively removed from MWNTs by introducing water vapor into the CVD furnace (*9*). Metal particles further stimulate oxidation of carbon [for example, carbon in contact with metal particles is removed at temperatures as low as 225°C (*5*)], and thus this effect should further assist the role of water as a protective agent against amorphous carbon coating. These results suggest that water-assisted growth could be applied to other growth systems, such as methane and acetylene CVD, or to grow other nanotubes, such as MWNTs. We believe that our understanding concerning the role of water represents a reasonable basic description, although future work is required to quantify and better understand the effect of water.

Realization of large-scale organized SWNT structures of desired shape and form is important for obtaining scaled-up functional devices. With the assistance of water, SWNTs grow easily from lithographically patterned catalyst islands into well-defined vertical-standing organized structures, as demonstrated by the large-scale arrays of macroscopic cylindrical pillars (Fig. 4A) with 150-μm radius, 250-μm pitch and a

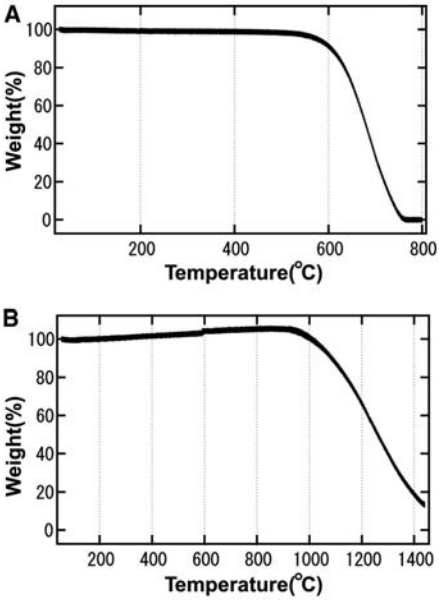

Fig. 2. Thermogravimetric properties of the SWNT material. (**A**) TGA data (ramp rate, 10°C/min) of a 10-mg sample of the SWNT material in air. (**B**) TGA data (ramp rate, 10°C/min) of a 9-mg sample of the SWNT material in N_2 (flow rate, 100 cc/min. standard temperature and pressure) passed through a water bubbler.

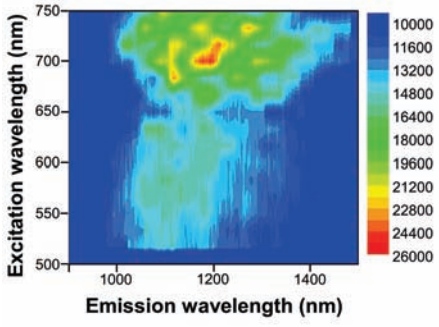

Fig. 3. Contour plot of fluorescence intensity versus excitation and emission wavelengths for the as-grown SWNT forest sample.

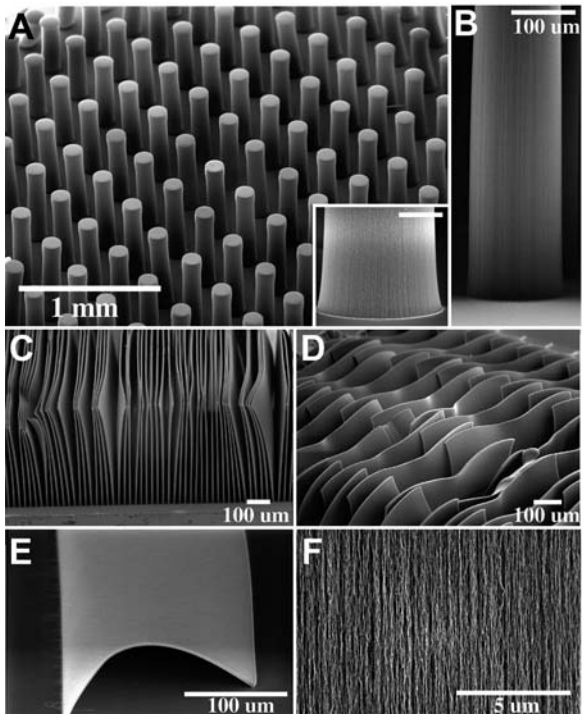

Fig. 4. SEM images of organized SWNT structures. (**A**) SEM image of SWNT cylindrical pillars with 150-μm radius, 250-μm pitch, and ~1-mm height. Inset, SEM image of a root of a pillar. Scale bar, 50 μm. (**B**) Side view of a pillar. Scale bar, 100 μm. (**C** and **D**) SEM images of SWNT sheets 10 μm thick. (**E**) SEM image of an isolated SWNT sheet 5 μm thick. (**F**) SEM image of the sheet face.

height close to 1 mm. A close examination (Fig. 4B) shows that the pillars are standing vertically from the substrate. Notably, the cross section of the SWNT structure corresponds well with the patterned catalyst (inset of Fig. 4A), and thus it is possible to fabricate arbitrary shapes of organized SWNT structures in which the base is lithographically defined and the height is controlled by the growth time. To further explore this unusual opportunity, we templated rows of catalytic stripe patterns and succeeded in growing pseudo two-dimensional organized SWNT structures (Fig. 4, C and D) that resemble sheets. A close investigation of a sheet face (Fig. 4F) reveals that the SWNTs are well aligned, with high uniformity. Some of these sheets are curved like pages in a book, which demonstrates their flexibility. This aspect is highlighted in Fig. 4E, in which an isolated thin SWNT sheet 5 μm thick was fabricated. Although this sheet formed a well-organized structure, its flexibility allowed it to bow and touch the surface, a point that suggests these thin sheets could be arbitrarily laid down, for example, by mechanical forces, gas flows, or electric fields.

Our approach is applicable to other synthesis methods developed for the mass production of SWNTs, such as rotary kiln, floating catalyst, and fluidized bed, addressing simultaneously such critical problems as scalability, purity, and cost. Thus, our approach represents an advance toward a realization of large-scale SWNT material. Additionally, our SWNTs are pure enough for use in various fields ranging from biology and chemistry to magnetic research. Highly pure SWNTs could be grown into scaled-up macroscopic organized structures with defined shape, be it a three-dimensional complex structure or a two-dimensional flexible sheet; potential applications include optical polarizers and field-emitter arrays for flat-panel displays.

References and Notes

1. S. Helveg *et al.*, *Nature* **427**, 426 (2004).
2. Material and methods are available as supporting material on *Science* Online.
3. H. Choi *et al.*, *Nano Lett.* **3**, 157 (2003).
4. M. Cinke *et al.*, *Chem. Phys. Lett.* **365**, 69 (2002).
5. W. I. Chiang *et al.*, *J. Phys. Chem. B* **105**, 8297 (2001).
6. M. J. O'Connell *et al.*, *Science* **297**, 593 (2002).
7. K. Tohji *et al.*, *Nature* **383**, 679 (1996).
8. K. Tohji *et al.*, *J. Phys. Chem. B* **101**, 1974 (1997).
9. A. Cao, X. Zhang, C. Xu, D. Wu, B. Wei, *J. Mater. Res.* **16**, 3107 (2001).
10. We thank Y. Kakudate for x-ray analyses, T. Yokoi for assistance with spectrofluorimetric measurements, K. Suenaga, K. Urita for some TEM observations, and T. Okazaki and M. Yudasaka for helpful discussions. Partial support by the New Energy and Industrial Technology Development Organization (NEDO) Nano Carbon Technology project and the use of the AIST Nano-Processing Facility are acknowledged.

Supporting Online Material

www.sciencemag.org/cgi/content/full/306/5700/1362/DC1
Materials and Methods
Figs. S1 and S2
Movie S1

7 September 2004; accepted 21 October 2004

Mars' South Polar Ar Enhancement: A Tracer for South Polar Seasonal Meridional Mixing

A. L. Sprague,[1]* W. V. Boynton,[1] K. E. Kerry,[1] D. M. Janes,[1] D. M. Hunten,[1] K. J. Kim,[2] R. C. Reedy,[2] A. E. Metzger[3]

The gamma ray spectrometer on the Mars Odyssey spacecraft measured an enhancement of atmospheric argon over southern high latitudes during autumn followed by dissipation during winter and spring. Argon does not freeze at temperatures normal for southern winter (~145 kelvin) and is left in the atmosphere, enriched relative to carbon dioxide (CO_2), as the southern seasonal cap of CO_2 frost accumulates. Calculations of seasonal transport of argon into and out of southern high latitudes point to meridional (north-south) mixing throughout southern winter and spring.

Between autumn (areocentric longitude of the Sun L_s 0° to 90°) (*1*) and winter in the southern hemisphere of Mars, about 25% of the atmosphere accumulates as a thick southern polar cap of CO_2 frost. Argon, a noncondensable gas, is left behind in the polar region (along with N_2, O_2, and CO) and becomes more enriched relative to CO_2, the main constituent in the atmosphere, as autumn progresses. The atmosphere near the poles tends to be isolated from the equatorial regions because of the conservation of angular momentum. If winds attempt to flow toward a pole, they are turned in the direction of the planet's rotation and form a vortex. This phenomenon has received attention in connection with the terrestrial polar ozone holes, the chemistry of which is connected to the isolation of the winter polar stratosphere and the special chemistry that takes place in this cold dark region. On Mars, very low temperatures above the southern polar winter night were discovered from analysis of Infrared Temperature Mapper measurements made from the Viking Orbiters (*2*, *3*). A substantial depletion in CO_2 might be the cause of the localized very low temperatures. Such a depletion would be accompanied by a large enhancement of the noncondensables Ar and N_2, and these were suggested to be enhanced by as much as a factor of 20 (*4*), particularly if CO_2 depletion was the cause of the localized cold spots. Here, we describe measurements of Ar in the polar region of the southern hemisphere.

Two of the three instruments comprising the gamma ray spectrometer (GRS) on Mars Odyssey (*5*–*7*) can study CO_2 frost accumulation and the cumulative effects of the sum of all noncondensables at southern latitudes by measuring the count rates of thermal neutrons, which show slightly lower values as noncondensables accumulate in the atmosphere (*8*). The GRS has the ability to measure Ar alone from the flux of the 1294-keV gamma ray associated with the 110-min half-life decay of Ar following neutron capture (*9*) [see supporting online material (SOM) text for details of this emission]. The instrument has a circular footprint on Mars with a diameter equal to about 240 km (*10*). We compute the fractional content of Ar relative to the total atmosphere in the polar region [mass mixing ratio (f_{GRS})] by dividing the mass of Ar measured by the GRS over the polar area by the mass of CO_2 in the polar atmosphere as predicted by the National Aeronautics and Space Administration Ames Research Center Mars Global Circulation Model (MGCM) run 2002.17 (*11*, *12*).

The relative Ar abundance (f_{GRS}) over Mars' southern polar latitudes from 75° to 90°S peaked at L_s 98°, 193 solar days (*13*) after CO_2 frost accumulation had begun (Fig. 1). The Ar abundance then decreased continuously throughout winter even though CO_2 frost accumulation continued. A minimum in Ar mass mixing ratio occurred after solid CO_2 began to sublime off the cap in early spring. Although the increase and decrease in Ar abundance are notable, the real surprise is that the data indicate transport of Ar equatorward throughout winter and poleward in spring. The Ar mixing ratio drops below the Viking Lander 2 (VL2) value (*14*) but is still measurable, despite rapid dilution

[1]Lunar and Planetary Laboratory, 1629 East University Boulevard, University of Arizona, Tucson, AZ 85721–0092, USA. [2]Institute of Meteoritics, MSC03-2050, University of New Mexico, Albuquerque, NM 87131–0001, USA. [3]Jet Propulsion Laboratory, Pasadena, CA 91109, USA.

*To whom correspondence should be addressed. E-mail: sprague@lpl.arizona.edu